The fine-scale signature of precipitation intensification trends in the CONUS-404 hydroclimate reanalysis between 1993 and 2022

Clement Guilloteau[1], Xiaodong Chen[2], L. Ruby Leung[3], and Efi Foufoula-Georgiou[4]

[1]University of California Irvine
[2]The University of Oklahoma
[3]Pacific Northwest National Laboratory
[4]University of California, Irvine

June 26, 2025

Abstract

Trends in annual precipitation statistics are extracted from the CONUS-404 hydroclimate reanalysis for the 1993-2022 period. For the annual precipitation volume, contrasted trends are found across CONUS, and most of them are statistically non-significant. When decomposing the annual precipitation volume into number of wet days and mean wet-day intensity, at 40-km resolution, the fraction of CONUS showing significant trends remains low. At 4-km and 1-hour resolution however, an intensification of the mean wet-hour precipitation intensity is found over 81% of CONUS, and the fraction of the domain showing significant increasing trends is three times greater than at 40-km daily resolution. This intensification of precipitation during wet hours is particularly pronounced in the Midwest. Changes in the multiscale spatial and temporal organization of precipitation are assessed through Fourier spectral analysis, revealing that the intensification of small-scale short-lived precipitation features occurs at a higher rate than that of larger-scale longer-persistence features.

Hosted file

Manuscript_CONUS_404_trends_V11.docx available at https://authorea.com/users/556947/articles/1306314-the-fine-scale-signature-of-precipitation-intensification-trends-in-the-conus-404-hydroclimate-reanalysis-between-1993-and-2022

The fine-scale signature of precipitation intensification trends in the CONUS-404 hydroclimate reanalysis between 1993 and 2022

Clément Guilloteau[1,*], Xiaodong Chen[2,3], L. Ruby Leung[4], and Efi Foufoula-Georgiou[1,5]

[1] Department of Civil and Environmental Engineering, University of California Irvine

[2] School of Meteorology, University of Oklahoma, Norman

[3] School of Civil Engineering and Environmental Science, University of Oklahoma, Norman

[4] Atmospheric, Climate and Earth Sciences Division, Pacific Northwest National Laboratory, Richland, Washington

[5] Department of Earth System Science, University of California Irvine

* corresponding author, cguillot@uci.edu

Key points

- Trends in daily precipitation statistics from 1993 to 2022 at 40-km resolution in CONUS-404 are mostly statistically non-significant.
- At the 4-km and 1-hour resolution, significant increasing trends are found in the mean wet-hour intensity, mostly in the Midwest.
- Spectral analysis shows that the magnitude of small-scale short-lived features has increased at a higher rate than that of larger features.

Abstract

Trends in annual precipitation statistics are extracted from the CONUS-404 hydroclimate reanalysis for the 1993-2022 period. For the annual precipitation volume, contrasted trends are found across CONUS, and most of them are statistically non-significant. When decomposing the annual precipitation volume into number of wet days and mean wet-day intensity, at 40-km resolution, the fraction of CONUS showing significant trends remains low. At 4-km and 1-hour resolution however, an intensification of the mean wet-hour precipitation intensity is found over 81% of CONUS, and the fraction of the domain showing significant increasing trends is three times greater than at 40-km daily resolution. This intensification of precipitation during wet hours is particularly pronounced in the Midwest. Changes in the multiscale spatial and temporal organization of precipitation are assessed through Fourier spectral analysis, revealing that the intensification of small-scale short-lived precipitation features occurs at a higher rate than that of larger-scale longer-persistence features.

Plain language summary

This study analyzes precipitation records covering the past three decades (1993 to 2022) over the Contiguous United States (CONUS) seeking trends in precipitation statistics. When performing the analysis at 40-km resolution, it is found that, over most of CONUS, the magnitude of the internal year-to-year variability dominates that of the long-term trends in terms of annual precipitation amount, annual number of wet days and mean intensity of wet days. When focusing however on the mean intensity of precipitation during wet hours at 4-km resolution, a clear intensification trend emerges over a large fraction of CONUS, in the Midwest in particular. Further analyses reveal that the average amplitude of short-lived small-size precipitation features has increased at a higher rate than that of large long-lived features.

1. Introduction

Increased atmospheric temperatures under global warming are expected to lead to increased atmospheric water content on average, as the Clausius-Clapeyron relationship establishes that the water-holding capacity of the atmosphere increases by 7% for every 1-K increase in temperature [North and Erukhimova 2009]. Change in atmospheric water content is ultimately expected to translate into changes in precipitation statistics, with increased precipitation volume on average. The response of precipitation characteristics to temperature changes is however strongly nonlinear, and, beyond the Clausius-Clapeyron relationship, precipitation patterns at the global, regional and local scales respond to changes in synoptic circulation patterns controlling moisture transport, and changes in the thermodynamics of precipitating cloud involving moist convection processes. For these reasons, historical precipitation trends across the globe generally show contrasting patterns [Zaitchik et al. 2023], and some studies have reported contradictory findings regarding the sign, magnitude, spatial patterns and statistical significance of precipitation trends [e.g., Emmanouil et al. 2022, Williams et al. 2024, Nerantzaki et al. 2025]. Moreover, global climate models often fail to accurately reproduce historical precipitation trends [Gu and Adler 2023], and are often inconsistent with each other regarding future projected precipitation trends [Li et al. 2021, John et al. 2022]. Yet, within these contrasted findings, a consensus emerges regarding high precipitation extremes, whose frequency and magnitude appear to increase consistently in both observations and model predictions, across different regions of the globe, different observational datasets, and different climate models [e.g., O'Gorman 2015, Papalexiou and Montanari 2019, Thackeray et al. 2022]. This increase in the frequency and magnitude of precipitation extremes is generally attributed to a shift toward a higher convective fraction and higher convective intensity in precipitating clouds in warmer climates and has been sometimes labelled as "super-Clausius–Clapeyron" scaling, as its magnitude can exceed the 7%-per-K rate of the Clausius-Clapeyron relationship [Haerter and Berg 2009, Berg et al. 2013, Panthou et al. 2014, Fowler et al. 2021, Da Silva and Haerter 2025].

The contiguous United States (CONUS) has been the focus of numerous studies seeking to identify trends in historical precipitation datasets [e.g. Feng et al. 2016, Hu et al. 2020]. For the recent decades, high-resolution reliable precipitation records are available over CONUS, which is unfortunately not the case for many other regions of the world (including, in particular, oceanic regions and the "Global South"). In the present study, precipitation statistics from the recently released CONUS-404 hydroclimate reanalysis [Rasmussen et al. 2023] are analyzed for the 1993-2022 period. The annual precipitation volume is first decomposed into number of wet days and mean wet-day intensity at the daily 40-km resolution, and then into number of wet hours and mean wet-hour intensity at the hourly 4-km resolution. The fraction of wet hours above increasing intensity thresholds is also assessed, and the spatial and temporal organization of precipitation features across scales is evaluated through the Fourier power spectral density (PSD) of the precipitation fields.

This study revisits the intensification of precipitation extremes and the super-Clausius-Clapeyron scaling paradigms from a scale-dependent perspective rather than an intensity-dependent perspective. We show that, when focusing on sub-daily kilometric precipitation statistics, the signature of the intensification of precipitation rates is detectable at a significant level in low-order statistics such as conditional means and scale-specific variances, and not only in the statistics of rare extreme events which have been the focus of numerous previous studies.

2. Data and method

2.1. The CONUS-404 downscaled hydroclimate reanalysis

The CONUS-404 high-resolution (4-km, 1-hour) hydroclimate reanalysis covering the 1980-2022 period has been released in December 2023 [Rasmussen et al. 2023]. This dataset results from the dynamical downscaling of the ECMWF ERA-5 global reanalysis [Hersbach et al. 2020] through the WRF model. At 4-km resolution WRF explicitly resolves mesoscale processes and orographic forcing. Compared to gridded precipitation estimation products derived from observations only (ground stations, precipitation radars, and satellite measurements), CONUS-404 has advantages in terms of resolution [Guilloteau et al. 2017, Guilloteau and Foufoula-Georgiou 2020] and consistency and homogeneity over space and time [Eldardiry et al. 2017, Carvalho 2020, Rasmussen et al. 2023]. When it comes to trend analysis at multi-decadal scales, the stability over time of the observation network becomes critical. For exclusively observation-derived products, technological evolutions of the sensors and the data processing chain, while allowing for improved estimation accuracy over time, are prone to introducing artifacts in the records [Petković et al. 2023]. Moreover, the number of sensors in an observational network often varies over time as well as the spatial distribution of the sensors and the temporal frequency of the observations, leading to inhomogeneous spatial and temporal sampling [Kidd et al. 2017, Ayat et al. 2021, Rajagopal et al. 2021]. While CONUS-404 is constrained by the observations assimilated in ERA-5, its fine-scale precipitation patterns essentially result from the thermodynamics of the WRF model, whose parametrization remains constant and homogeneous over the simulated period. CONUS-404 therefore inherits the advantages of numerical models in terms of homogeneity and consistency over time and space, while still relying on observations for its boundary conditions, allowing for realistic synoptic forcing and sub-seasonal to decadal variability and mitigating model biases [Rasmussen et al. 2023].

In this study the CONUS-404 data from 1993 to 2022 is analyzed. Limiting the analysis to the post-90's era allows to limit the potential influence of data artifacts in ERA-5 in the early years of the satellite era [Buschow 2024, Bromwich et al. 2024], as well as data artifacts in the first six years of the CONUS-404 record (1980-1985), due to spinup issues with the WRF downscaling model [Rasmussen et al. 2023].

2.2. Linear trend extraction through least squares regression

In this study, precipitation statistics over the 1993-2022 period are first analyzed in terms of annual number of wet days (or wet hours) and mean annual wet-day (or wet-hour) intensity. A wet day (or wet hour) is defined as a day (or hour) with at least 0.1 mm of accumulated precipitation. The mean annual wet-day (or wet-hour) intensity is the mean precipitation intensity over all the wet days (or wet hours) of the year. The annual number of wet days and mean annual wet-day intensity are computed at the 40-km spatial resolution. The annual number of wet hours and mean annual wet-hour intensity are computed at the 4-km spatial resolution and then averaged spatially at the 40-km scale. This is done to assess scale-dependence in the magnitude and statistical significance of precipitation trends. The land areas of the CONUS-404 domain are divided into 7477 surface elements ("surfels") of dimensions 40 km by 40 km. In each surfel, the 1993-2022 series of annual precipitation volume, number of wet days, number of wet hours, mean wet-day intensity mean annual wet-hour intensity are constructed and linear trends are extracted by least squares regression of the annual values $X(y)$ against the year y. The regressed line $\bar{X}(y)$ follows the equation:

$$\bar{X}(y) = 0.1\, \alpha\, (y - 1993) + \beta$$

The regressed trends are characterized by the slope coefficient α, expressed in $mm\, dec^{-1}$ when X represents precipitation volume or intensity, or in dec^{-1} when X represents the number of wet days (or wet hours). In the following, the relative slope coefficient α' in percent per decade is often used instead of the absolute slope coefficient α to characterize the trends:

$$\alpha' = \frac{\alpha}{\hat{X}_{D1}}$$

where $\hat{X}_{D1}$ represents the mean value of the variable of interest over the first decade of the analysis period (1993-2002).

In each surfel and for each variable of interest the p-value of the trend has been estimated with three different methods: t-test, Mann-Kendall test and Monte Carlo permutations. As the three methods produced highly-consistent p-values (see supplementary material) only t-test-derived p-values are reported below. Trends with p-value lower than 0.05 are considered statistically significant.

2.3. Statistical distribution of precipitation intensities

The statistical distributions of wet-hour precipitation intensities at 4-km resolution are represented through probability of exceedance (PoE) curves. PoE curves are advantageous when focusing on the tail of the distribution and the rare extreme events. To quantitatively represent the change in the distribution between the first decade of the analysis period (D1, 1993-2002) and the last decade (D3, 2013-2022), the ratio of the respective PoE curves is shown. If, for an intensity value R, the PoE ratio $\frac{\mathrm{PoE}_{D3}(R)}{\mathrm{PoE}_{D1}(R)} = \gamma$, then the probability of exceeding the intensity value R has been multiplied by γ between the first decade and the last decade.

Changes in the distribution between the D1 and D3 are also represented through the quantile-quantile plots, specifically, through the $\frac{Q_{D3}(F)}{Q_{D1}(F)}$ ratio, where the quantile function $Q(F)$ is the inverse of the cumulative density function (CDF) with F in $[0,1]$.

2.4. Spatial and temporal Fourier power spectral densities

The space-time dynamics of the 1-hour 4-km precipitation fields are analyzed through their spatial and temporal Fourier power spectral densities (PSDs). The temporal PSDs of the hourly precipitation time series are computed in each 4-km pixel of the CONUS-404 dataset and are then spatially averaged over specific regions of interest. The two-dimensional spatial PSDs are computed from the 4 km precipitation maps in pre-defined regions of interest for each hour of the 1993-2022 period, and are then temporally averaged over specific periods of interest. The two-dimensional spatial power spectra, defined in polar coordinates as functions of the spatial wavenumber and the azimuthal direction, are subsequently averaged over all azimuthal directions to produce the omnidirectional spatial PSD as a univariate function of the spatial wavenumber. For easier interpretation, the spatial and temporal PSDs are shown as functions of temporal period and spatial wavelength, respectively, instead of frequency and wavenumber.

Changes in the spatial and temporal PSDs between D1 and D3 are represented through the ratio of the PSDs.

3. Results

3.1 Trends in precipitation occurrence and intensity at different spatio-temporal scales over CONUS

Wet days are defined as days with at least 0.1 mm of cumulative precipitation (section 2.2). If we ignore the contribution of days with precipitation amounts between 0.0 and 0.1 mm, the annual precipitation volume can be calculated as the product of the number of wet days by the mean wet-day intensity. Relative trends in the annual precipitation volume, number of wet days and mean wet-day intensity are reported in Figure 1 for each one of the 7477 surfels (40 km by 40 km) of the study domain.

For the annual precipitation volume, 68% of the surfels show a positive trend and 32% a negative trend. Negative trends are essentially found in the West; positive trends are found in the South (northern Mexico), North (southern Canada) and East. However, when considering solely statistically significant trends (p-value < 0.05), only 5.6% of the surfels show a significant positive trend and 4.4% a significant negative trend (and 89% of the surfels do not show statistically significant trends). Even the strong negative trends (-10% to -15% per decade) in the West are deemed not statistically significant in most surfels because of the strong year-to-year variability of the precipitation volume in this region.

When decomposing the annual precipitation volume into the number of wet days and mean wet-day intensity, it appears that the decreasing precipitation volume trend in the West essentially reflects a decrease in the number of wet days. In contrast, the increasing volume trends in the South, North and East are associated with an increase of wet-day intensity, with little variation in the number of wet days. Most of these trends are however not statistically significant, only 4.2% of the surfels show a statistically significant trend in the number of wet days and 5.8% in the mean wet-day intensity, when 5% spurious significant trends are expected on average for a 0.05 p-value under the null hypothesis.

The top row of Figure 2 shows trends in precipitation occurrence and intensity when computing statistics at the 1-hour and 4-km resolution instead of 24 hours and 40 km. Trends in the number of wet hours essentially show a decrease in the West which is deemed non-significant (only 1.1% of the surfels show a significant decreasing trend, which is less than what is expected on average under the null hypothesis). Most interestingly, at the 1-hour and 4-km resolution, 81% of the surfels of CONUS show an increase in the mean wet-hour intensity, and 15% show a statistically significant increase (6 times more than what would be expected under the null hypothesis). The fractional area of CONUS showing a statistically significant increase of the mean wet-hour intensity at 4-km resolution is nearly three times larger than the fractional area showing a statistically significant increase of the mean wet-day intensity at the 40-km resolution. The increasing wet-hour intensity trends with the greatest magnitude (+5% to +15% per decade) are found in the Midwest.

For this study, we define the Midwest as the longitudes between -108° and -80° and latitudes between 38° and 49° (Figure 2, top-right panel), and focus on this region for further analysis of precipitation trends. The bottom left panel of Figure 2 shows the 1993-2022 time series of the annual mean wet-hour precipitation intensity at 4-km resolution in the Midwest. The wet-hour intensity increases at an average rate of $0.04\ mm\ h^{-1}\ dec^{-1}$ over the Midwest, which corresponds to a $4\%\ dec^{-1}$ increase with respect to the 1993-2002 average wet-hour intensity. This spatially-averaged trend in the Midwest is statistically significant with a p-value of 6×10^{-5}.

To assess changes in the distribution of wet-hour intensities beyond the mean, we analyze the fraction of wet hours with intensities above pre-defined thresholds. Three thresholds are used, defined in each surfel of the CONUS domain as $2 \times \hat{R}_{D1}$, $4 \times \hat{R}_{D1}$ and $8 \times \hat{R}_{D1}$, where $\hat{R}_{D1}$ is the average wet-hour intensity during the first decade of the analysis (1993-2002) in the corresponding surfel. These intensity thresholds are considered as medium-high intensities, high intensities and extreme intensities respectively. The second row of Figure 2 shows the 1993-2022 relative trends in the fraction of wet hours with intensities above the medium-high-, high-, and extreme-intensity thresholds, over each 40 km by 40 km surfel. While the spatial patterns of the trends are similar for the different thresholds, and generally follow the spatial pattern of the mean wet-hour intensity trends, we note that, the higher the threshold, the greater the relative magnitude of the increasing trends, with locally up to a +30% per decade increase of the fraction of wet hours above $8 \times \hat{R}_{D1}$. In the Midwest region, the fraction of wet hours above the extreme intensity threshold is found to have increased at an average rate of +12% per decade (with respect to the 1993-2002 mean fraction) over the 1993-2022 period (bottom right panel of Figure 2).

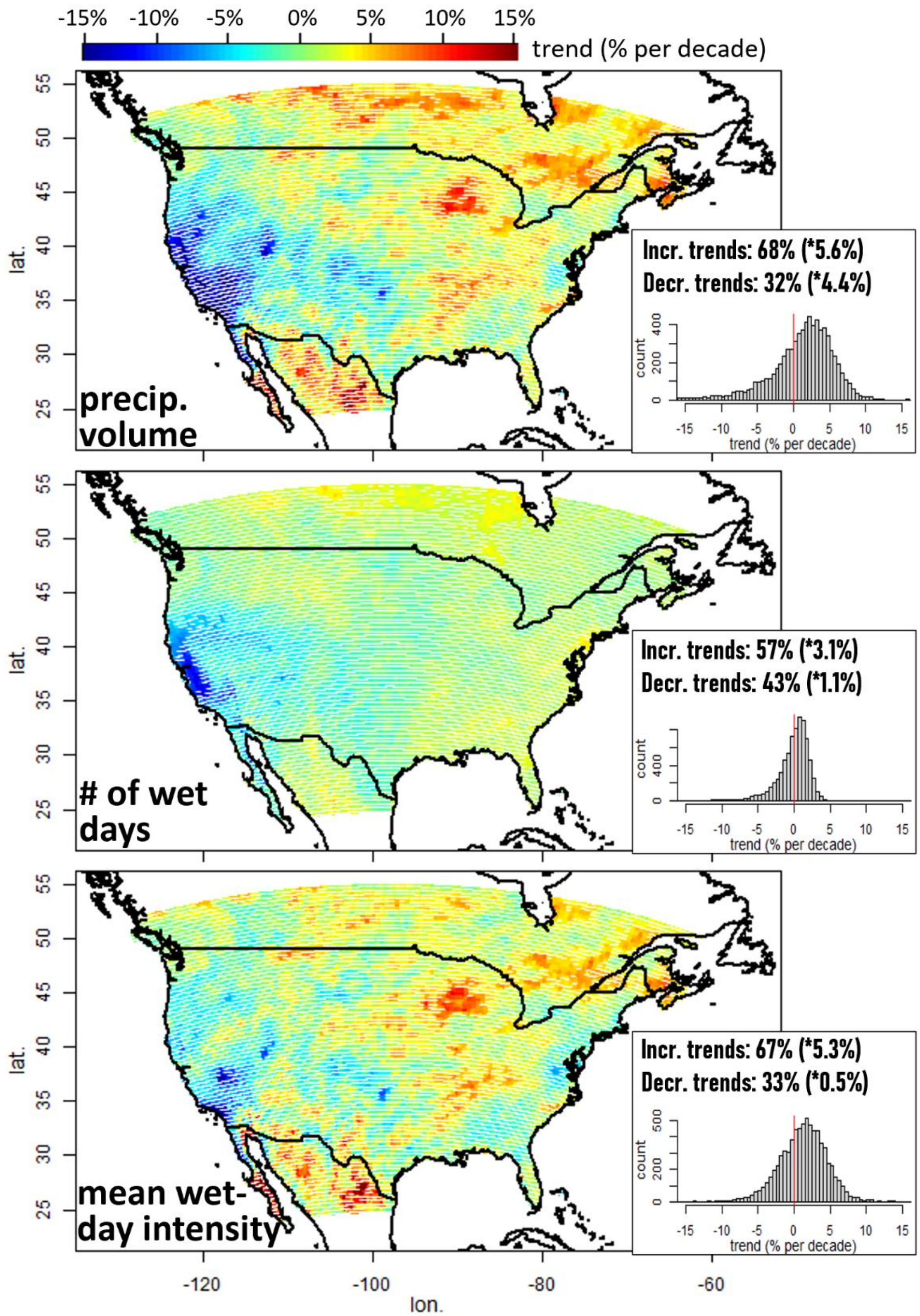

Figure 1: Maps of the relative trends in annual precipitation volume, number of wet days and mean wet-day intensity for the 1993-2022 period. The white hatching indicates areas where trends are not significant at the 0.05 level. The histogram associated with each map shows the statistical distribution of the relative trends across the 7477 surfels of dimension 40 km by 40 km of the study domain. The

fractions of increasing and decreasing trends are indicated on top of the histograms, the fractions of statistically significant increasing and decreasing trends are indicated in parentheses. The relative trends are shown in % per decade, with respect to the average value over the first decade of the analysis period (1993-2002).

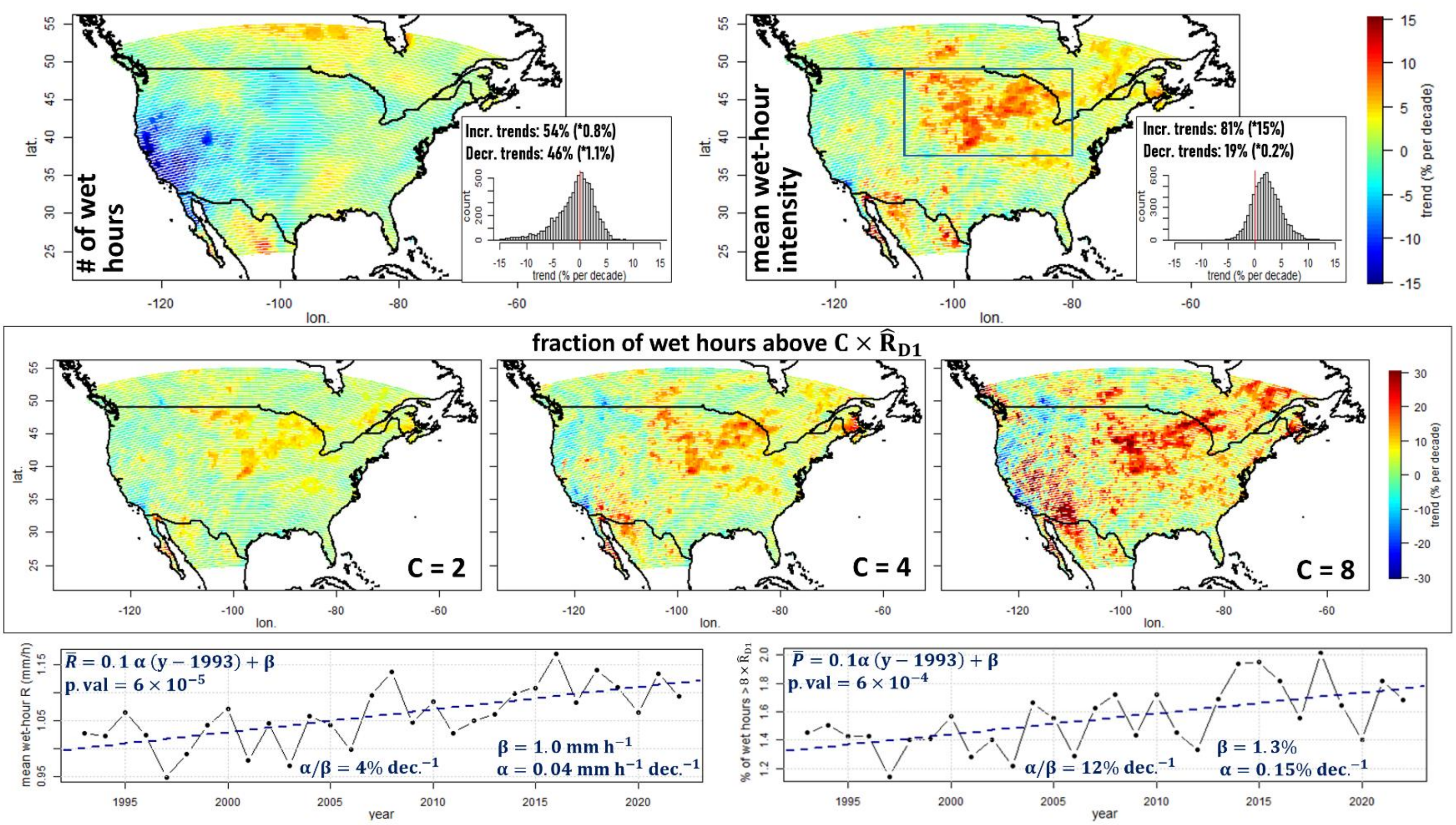

Figure 2: (Top row) Maps of the relative trends in number of wet hours and mean wet-hour intensity for the 1993-2022 period. The white hatching indicates areas where trends are not significant at the 0.05 level. The histogram associated with each map shows the statistical distribution of the relative trends across the 7477 surfels of dimension 40 km by 40 km of the study domain. The fractions of increasing and decreasing trends are indicated on top of the histograms, the fractions of statistically significant increasing and decreasing trends are indicated in parentheses. (Middle row) Maps of the relative trends in the fraction of wet hours with intensity above $2 \times \hat{R}_{D1}$, $4 \times \hat{R}_{D1}$ and $8 \times \hat{R}_{D1}$ respectively, for the

1993-2022 period, where $\hat{R}_{D1}$ is, for each surfel, the mean wet-hour intensity during the first decade of the analysis period. (Bottom row, left) Time series of the annual mean wet-hour intensity in the Midwest region with regressed linear trend for the 1993-2022 period. (Bottom row, right) Time series of the annual fraction of wet hours with intensity above $8 \times \hat{R}_{D1}$ in the Midwest region with regressed linear trend for the 1993-2022 period. The Midwest region corresponds to the blue rectangle in the top-right panel.

3.2 Statistical distribution of 4-km hourly precipitation intensities in the Midwest: 2013-2022 decade vs 1993-2002 decade

In this section, we further analyze changes in the statistical distribution of the 4-km wet-hour intensities in the Midwest, by comparing the statistics for the first decade of the analysis period (D1, 1993-2002) with the statistics for the last decade (D3, 2013-2022). The first row of Figure 3 shows a comparison of the respective PoE curves for the two decades, as well as the $\frac{\mathrm{PoE}_{D3}}{\mathrm{PoE}_{D1}}$ ratio as a function of intensity and the $\frac{Q_{D3}(F)}{Q_{D1}(F)}$ ratio as a function of $Q_{D1}(F)$. One can see that, the greater the intensity, the greater the difference between the D3 PoE and the D1 PoE. Between the 0.1 mm/h and 1 mm/h intensities the PoE ratio remains relatively close to 1, revealing that the distribution remained relatively stable for low intensities. At intensity 10 mm/h, the D3 PoE is 1.25 times greater than the D1 PoE (+25% increase). At intensity 50 mm/h the increase in the PoE between the two decades is +55%.

The Q/Q ratio plot reveals that the increase in the wet-hour intensities is not linear, meaning that the D3 distribution cannot be obtained by linearly scaling the D1 intensity values with a constant coefficient. If this were the case the Q/Q ratio curve would be flat. The Q/Q ratio curve is found to increase with quantile values up to the 99th percentile (Q99%) at which it reaches a peak value of 1.13, meaning that the intensity value associated with the 99th percentile of the distribution of wet-hour intensities is 13% greater for D3 than for D1. This non-linear increase of precipitation intensities, intensity values increasing at a higher rate for higher values is consistent with what has been reported in the literature for CONUS and in other regions of the globe [Feng et al. 2016, Fowler et al. 2021]; we note however that, in our case, this holds only up to the 99th percentile, corresponding to intensities of the order of 10 mm/h.

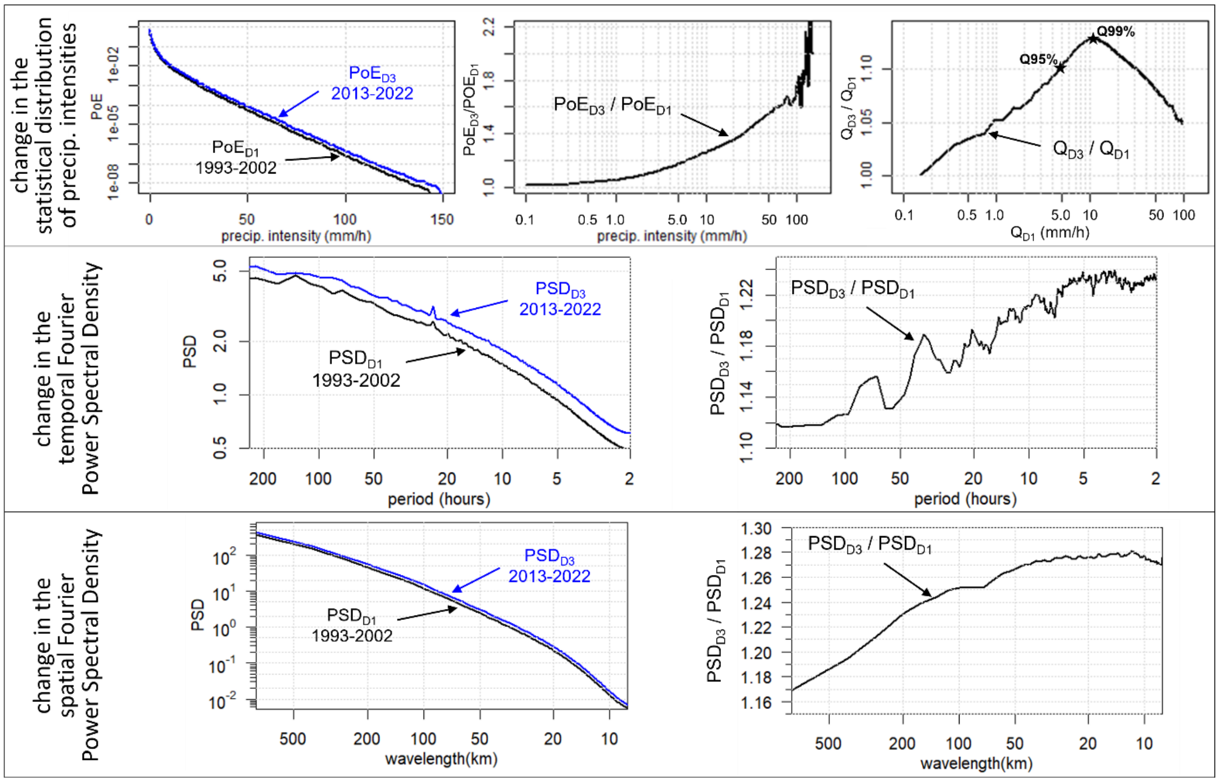

Figure 3: Comparison of precipitation statistics at 1-hour and 4-km resolution in the Midwest between the 1993-2002 decade (D1) and the 2013-2022 decade (D3). (Top row, left) Probability of exceedance (PoE) as a function of the wet-hour intensity R, for D1 (black curve) and D3 (blue curve). (Top row, middle) PoE ratio curve $\frac{\mathrm{PoE}_{D3}(R)}{\mathrm{PoE}_{D1}(R)}$. (Top row, right) Quantile to quantile ratio $\frac{Q_{D3}(F)}{Q_{D1}(F)}$ as a function of $Q_{D1}(F)$, where $Q_{D1}(F)$ and $Q_{D3}(F)$ are the quantile functions of the distribution of wet-hour intensities for D1 and D3 respectively. The 95th and 99th percentiles are marked on the curve (Q95% and Q99%). (Middle row, left) Temporal Fourier power spectral density functions (PSD) of the hourly precipitation time series, for D1 (black curve) and D3 (blue curve). (Middle row, right) PSD ratio $\frac{\mathrm{PSD}_{D3}(p)}{\mathrm{PSD}_{D1}(p)}$ as a function of the temporal period p. (Bottom row, left) Omnidirectional spatial Fourier power spectral density functions (PSD) of the hourly precipitation maps, for D1 (black curve) and D3 (blue curve). (Bottom row, right) PSD ratio $\frac{\mathrm{PSD}_{D3}(\lambda)}{\mathrm{PSD}_{D1}(\lambda)}$ as a function of the spatial wavelength λ.

3.3 Spatial and temporal spectral characteristics of precipitation in the Midwest: 2013-2022 decade vs 1993-2002 decade

In this section, changes in the space-time dynamics of precipitation are quantified through temporal and spatial Fourier spectral analyses of the 1-hour 4-km precipitation intensity fields. The spatial and temporal Fourier PSD functions allow us to non-parametrically detect and quantify changes in space-time dynamics of precipitation [Guilloteau et al. 2025], at a minimal computational cost using a fast Fourier transform algorithm.

Here also, the statistics for the 2013-2022 decade (D3) are compared to that of the 1993-2002 decade (D1), in the Midwest. One can see that, at all Fourier periods and wavelengths, the D3 PSD is higher than the D1 PSD (the $\frac{PSD_{D3}}{PSD_{D1}}$ ratio is greater than 1), reflecting an overall increase of the variability (variance) of the 1-hour 4-km precipitation intensities between D1 and D3, across all spatial and temporal scales (Figure 3, second and third row). Interestingly, the magnitude of the PSD increase between D1 and D3 is greater at shorter periods and shorter wavelengths, revealing that the average amplitude of short-lived small-size precipitation features has increased at a higher rate than that of large long-lived features. Specifically, as the Fourier period get shorter, the $\frac{PSD_{D3}}{PSD_{D1}}$ ratio gets larger, from a 1.12 value (meaning a +12% increase of the PSD between D1 and D3) at periods longer than 100 hours, down to the 6-hour period at which the PSD ratio reaches a plateau around a value of 1.23 (+23% increase of the PSD between D1 and D3). The $\frac{PSD_{D3}}{PSD_{D1}}$ ratio also gets larger with shorter Fourier wavelengths, down to the 50-km wavelength, where it plateaus between 1.27 and 1.28 (+27% to +28% increase of the PSD between D1 and D3). This again demonstrates a scale-dependence in the magnitude of the change in precipitation statistics, the changes becoming more pronounced at finer spatial and temporal scales. The PSD having increased at a higher rate at shorter periods and shorter wavelengths also corresponds to a decrease of the spectral slope (slope of the PSD curves) between D1 and D3, which, in precipitation data, is generally interpreted as a signature of increasing convective activity and atmospheric instability [Harris et al. 2001, Willeit et al. 2015].

4. Conclusions

The analysis of precipitation statistics in the CONUS-404 downscaled hydroclimate reanalysis at 4-km and 1-hour resolution shows a clear increase of mean precipitation intensity during wet hours for the 1993-2022 period, over most of the CONUS domain, and in particular in the Midwest where the average rate of increase is $+0.04\, mm\, h^{-1}\, dec^{-1}$ ($+4\%\, dec^{-1}$ with respect to the 1993-2002 mean wet-hour intensity). This rate of increase is largely above what is predicted by the Clausius-Clapeyron relationship, given that trends in mean annual atmospheric temperature reported in the literature are of the order of 0.1 to 0.25 $K\, dec^{-1}$ for the recent decades in the Midwest [U.S. Global Change Research Program 2023].

The nonlinear scaling of precipitation intensities between the first decade and the last decade of the analysis period in the Midwest, and the changes in the space-time structure of precipitation fields revealed by the changes in the temporal and spatial Fourier PSD indicate a change in precipitation dynamics, consistent with the hypothesis of a shift toward a higher convective fraction and higher convective intensity of precipitating clouds. It is not surprising that the signature of this shift is clearly perceptible in the precipitation statistics at high resolution (e.g., 1 hour and 4 km) but is fainter at coarser resolutions (e.g., 24 hours and 40 km). Indeed, a long-lived large-extent medium-intensity stratiform precipitating system may produce the same amount of precipitation as a more localized and short-lived high-intensity convective system; however, these two systems would undoubtedly show radically different space-time variability and statistical distribution of precipitation intensities at a fine scale. As compared to stratiform clouds, convective cloud systems tend to produce more intense precipitation over shorter periods of time and more concentrated areas, the amplification of short-period and short-wavelength precipitation features revealed by the Fourier spectral analysis is thus also consistent with a shift toward more frequent and more intense convective precipitation.

We note that it is only when convection becomes organized at a large scale, forming mesoscale convective systems (MCSs) or mesoscale convective complexes through the aggregation of several convective cells, and causing widespread high-intensity precipitation over periods exceeding 12 hours [Feng et al. 2016, Hu et al. 2020, Schumacher and Rasmussen 2020], that convective precipitation may become statistically distinguishable from stratiform precipitation at coarse resolution. Notably, the statistical signature of organized MCSs is identifiable at coarse resolutions (24 hours and 40 km or coarser) [Roca et al. 2014, Roca and

Fiolleau 2020, Zhao 2022], unlike that of isolated short-lived convective cells. For this reason, historical multi-decadal changes in precipitation statistics at coarse resolution may only be noticeable when focusing on organized MCSs, which are generally associated with extreme high values in daily-accumulated precipitation amounts at 40 km to 100 km resolutions. This may explain why studies reporting historical trends in precipitation statistics at relatively coarse resolutions have often focused on high extremes, for which the changes may appear more pronounced [e.g., Papalexiou and Montanari 2019, Harrison et al. 2019, Alexander et al. 2020, Sun et al. 2021, Thackeray et al. 2022, Wang et al. 2023]. One must however consider that identifying trends in the frequency of extreme events with long return periods in a robust manner necessarily requires correspondingly long data records. In addition, observational data records often exhibit large biases and uncertainties when it comes to the representation of extremes, related to sensor limitations and data processing [Masunaga et al. 2019, Guilloteau and Foufoula-Georgiou 2023]. In the present study statistically significant trends and changes are identified not only in the frequency of extremes, but also in the mean intensity of precipitation during wet hours at the 4-km resolution and in the overall space-time dynamics of precipitation fields represented by the spatial and temporal Fourier PSD functions.

It is also worth noting that the nature of the statistical changes reported in the present analysis of historical data over CONUS, i.e., an increase of the mean wet-hour intensity and an amplification of the fine-scale variability of precipitation, over the Midwest in particular, is consistent with the changes reported in Guilloteau et al. [2025] between historical (1981-2020) and future (2041-2080) hydroclimate simulations at 6-km and 1-hour resolution over the western half of CONUS under the RCP8.5 scenario, and with other published studies focusing on future hydroclimate simulations [e.g. Westra et al. 2014, Dallan et al. 2024]. The present study tends to indicate that the hypothesized shift toward higher convective fraction and higher convective intensity in precipitating clouds under global warming, which has been confirmed by model simulations [Singleton and Toumi 2013, Moseley et al. 2016], is already detectable in high-resolution historical datasets in certain regions of the world. Such trends may however be less detectable at the coarse resolutions of global products (observational products and reanalysis) and global climate models.

Acknowledgements

This work was supported by NASA (grants 80NSSC22K0597 and 80NSSC23K1304), the National Science Foundation (grant IIS2324008), and by the Office of Science of the U.S. Department of Energy through the HyperFACETS project within the Regional and Global Model Analysis and Multisector Dynamics program. The Pacific Northwest National Laboratory is operated for the Department of Energy by the Battelle Memorial Institute under contract DE-AC05-76RL01830.

Data Availability statement

The CONUS-404 dataset (doi:10.5065/ZYY0-Y036) used in the present study is publicly available on the NSF NCAR Research Data Archive (https://oidc.rda.ucar.edu/datasets/d559000/).

References:

Alexander, L.V., Bador, M., Roca, R., Contractor, S., Donat, M.G. and Nguyen, P.L., 2020. Intercomparison of annual precipitation indices and extremes over global land areas from in situ, space-based and reanalysis products. Environmental Research Letters, 15(5), p.055002, doi: 10.1088/1748-9326/ab79e2

Ayat, H., Evans, J.P. and Behrangi, A., 2021. How do different sensors impact IMERG precipitation estimates during hurricane days?. Remote Sensing of Environment, 259, p.112417, doi:10.1016/j.rse.2021.112417

Berg, P., Moseley, C. and Haerter, J.O., 2013. Strong increase in convective precipitation in response to higher temperatures. Nature Geoscience, 6(3), pp.181-185, doi:10.1038/ngeo1731

Buschow, S., 2024. Tropical convection in ERA5 has partly shifted from parameterized to resolved. Quarterly Journal of the Royal Meteorological Society, 150(758), pp.436-446, doi:10.1002/qj.4604

Bromwich, D.H., Ensign, A., Wang, S.H. and Zou, X., 2024. Major artifacts in ERA5 2-m air temperature trends over Antarctica prior to and during the modern satellite era. Geophysical Research Letters, 51(21), p.e2024GL111907, doi:10.1029/2024GL111907

Carvalho, L.M., 2020. Assessing precipitation trends in the Americas with historical data: A review. Wiley Interdisciplinary Reviews: Climate Change, 11(2), p.e627, doi:1 0.1002/wcc.627

Dallan, E., Marra, F., Fosser, G., Marani, M. and Borga, M., 2024. Dynamical factors heavily modulate the future increase of sub-daily extreme precipitation in the alpine-mediterranean region. Earth's Future, 12(12), p.e2024EF005185, doi:0.1029/2024EF005185

Da Silva, N.A. and Haerter, J.O., 2025. Super-Clausius–Clapeyron scaling of extreme precipitation explained by shift from stratiform to convective rain type. Nature Geoscience, doi:10.1038/s41561-025-01686-4

Eldardiry, H., Habib, E., Zhang, Y. and Graschel, J., 2017. Artifacts in Stage IV NWS real-time multisensor precipitation estimates and impacts on identification of maximum series. Journal of Hydrologic Engineering, 22(5), p.E4015003, doi:10.1061/(ASCE)HE.1943-5584.000129

Emmanouil, S., Langousis, A., Nikolopoulos, E.I. and Anagnostou, E.N., 2022. The spatiotemporal evolution of rainfall extremes in a changing climate: A CONUS-wide assessment based on multifractal scaling arguments. Earth's Future, 10(3), p.e2021EF002539, doi:10.1029/2021EF002539

Feng, Z., Leung, L.R., Hagos, S., Houze, R.A., Burleyson, C.D. and Balaguru, K., 2016. More frequent intense and long-lived storms dominate the springtime trend in central US rainfall. Nature communications, 7(1), p.13429, doi:10.1038/ncomms13429

Fowler, H.J., Lenderink, G., Prein, A.F., Westra, S., Allan, R.P., Ban, N., Barbero, R., Berg, P., Blenkinsop, S., Do, H.X. and Guerreiro, S., 2021. Anthropogenic intensification of short-duration rainfall extremes. Nature Reviews Earth & Environment, 2(2), pp.107-122, 10.1038/s43017-020-00128-6

Gu, G. and Adler, R.F., 2023. Observed variability and trends in global precipitation during 1979–2020. Climate Dynamics, 61(1), pp.131-150, doi:10.1007/s00382-022-06567-9

Guilloteau, C., Foufoula-Georgiou, E. and Kummerow, C.D., 2017. Global multiscale evaluation of satellite passive microwave retrieval of precipitation during the TRMM and GPM eras: Effective resolution and regional diagnostics for future algorithm development. Journal of Hydrometeorology, 18(11), pp.3051-3070, doi:10.1175/JHM-D-17-0087.1

Guilloteau, C. and Foufoula-Georgiou, E., 2020. Multiscale evaluation of satellite precipitation products: Effective resolution of IMERG. Satellite Precipitation Measurement: Volume 2, pp.533-558, doi:10.1007/978-3-030-35798-6_5

Guilloteau, C. and Foufoula-Georgiou, E., 2023. Preserving Extremes in Satellite Quantitative Precipitation Estimates: A Matter of Scale. Proceedings of the IGARSS 2023 IEEE International Geoscience and Remote Sensing Symposium, pp. 662-665. doi:10.1109/IGARSS52108.2023.10281499

Guilloteau, C., Chen, X., Leung, L.R. and Foufoula-Georgiou, E., 2025. Amplified Mesoscale and Submesoscale Variability and Increased Concentration of Precipitation under Global Warming over Western North America. Journal of Climate, 38(11), pp.2525-2542, doi:10.1175/JCLI-D-24-0343.1

Haerter, J.O. and Berg, P., 2009. Unexpected rise in extreme precipitation caused by a shift in rain type?. Nature Geoscience, 2(6), pp.372-373, doi:10.1038/ngeo523

Harris, D., Foufoula-Georgiou, E., Droegemeier, K.K. and Levit, J.J., 2001. Multiscale statistical properties of a high-resolution precipitation forecast. Journal of Hydrometeorology, 2(4), pp.406-418, doi:10.1175/1525-7541(2001)002<0406:MSPOAH>2.0.CO;2

Harrison, L., Funk, C. and Peterson, P., 2019. Identifying changing precipitation extremes in Sub-Saharan Africa with gauge and satellite products. Environmental Research Letters, 14(8), p.085007, doi:10.1088/1748-9326/ab2cae

Hersbach, H., Bell, B., Berrisford, P., Hirahara, S., Horányi, A., Muñoz-Sabater, J., Nicolas, J., Peubey, C., Radu, R., Schepers, D. and Simmons, A., 2020. The ERA5 global reanalysis. Quarterly journal of the royal meteorological society, 146(730), pp.1999-2049, doi:10.1002/qj.3803

Hu, H., Leung, L.R. and Feng, Z., 2020. Observed warm-season characteristics of MCS and non-MCS rainfall and their recent changes in the central United States. Geophysical Research Letters, 47(6), p.e2019GL086783, doi:10.1029/2019GL086783

John, A., Douville, H., Ribes, A. and Yiou, P., 2022. Quantifying CMIP6 model uncertainties in extreme precipitation projections. Weather and Climate Extremes, 36, p.100435, doi: 10.1016/j.wace.2022.100435

Kidd, C., Becker, A., Huffman, G.J., Muller, C.L., Joe, P., Skofronick-Jackson, G. and Kirschbaum, D.B., 2017. So, how much of the Earth's surface is covered by rain gauges?. Bulletin of the American Meteorological Society, 98(1), pp.69-78, doi:10.1175/BAMS-D-14-00283.1

Li, J., Huo, R., Chen, H., Zhao, Y. and Zhao, T., 2021. Comparative assessment and future prediction using CMIP6 and CMIP5 for annual precipitation and extreme precipitation simulation. Frontiers in Earth Science, 9, p.687976, doi:10.3389/feart.2021.687976

Masunaga, H., Schröder, M., Furuzawa, F.A., Kummerow, C., Rustemeier, E. and Schneider, U., 2019. Inter-product biases in global precipitation extremes. Environmental Research Letters, 14(12), p.125016, doi:10.1088/1748-9326/ab5da9

Moseley, C., Hohenegger, C., Berg, P. and Haerter, J.O., 2016. Intensification of convective extremes driven by cloud–cloud interaction. Nature Geoscience, 9(10), pp.748-752, doi:10.1038/ngeo2789

Nerantzaki, S.D., Abdelmoaty, H.M., Papalexiou, S.M. and Newman, A.J., 2025. The influence of atmospheric drivers, environmental factors, and urban land use on extreme hourly precipitation trends over the CONtiguous United States for 40 years at 4-km resolution (CONUS404). Science of the Total Environment, 969, p.178407, doi:10.1029/2021EF002539

North, G.R. and Erukhimova, T.L., 2009. Chap. 9: Air and water. In Atmospheric thermodynamics: elementary physics and chemistry. Cambridge University Press, pp. 99-133.

O’Gorman, P.A., 2015. Precipitation extremes under climate change. Current climate change reports, 1, pp.49-59, doi:10.1007/s40641-015-0009-3

Panthou, G., Mailhot, A., Laurence, E. and Talbot, G., 2014. Relationship between surface temperature and extreme rainfalls: A multi-time-scale and event-based analysis. Journal of hydrometeorology, 15(5), pp.1999-2011, doi:10.1175/JHM-D-14-0020.1

Papalexiou, S.M. and Montanari, A., 2019. Global and regional increase of precipitation extremes under global warming. Water Resources Research, 55(6), pp.4901-4914, doi:10.1029/2018WR024067

Petković, V., Brown, P.J., Berg, W., Randel, D.L., Jones, S.R. and Kummerow, C.D., 2023. Can We Estimate the Uncertainty Level of Satellite Long-Term Precipitation Records?. Journal of Applied Meteorology and Climatology, 62(8), pp.1069-1082.

Rajagopal, M., Zipser, E., Huffman, G., Russell, J. and Tan, J., 2021. Comparisons of IMERG version 06 precipitation at and between passive microwave overpasses in the tropics. Journal of Hydrometeorology, 22(8), pp.2117-2130, doi:10.1175/JHM-D-20-0226.1

Rasmussen, R.M., Chen, F., Liu, C.H., Ikeda, K., Prein, A., Kim, J., Schneider, T., Dai, A., Gochis, D., Dugger, A. and Zhang, Y., 2023. CONUS404: The NCAR–USGS 4-km long-term regional hydroclimate reanalysis over the CONUS. Bulletin of the American Meteorological Society, 104(8), pp.E1382-E1408, doi:10.1175/BAMS-D-21-0326.1

Roca, R., Aublanc, J., Chambon, P., Fiolleau, T. and Viltard, N., 2014. Robust observational quantification of the contribution of mesoscale convective systems to rainfall in the tropics. Journal of Climate, 27(13), pp.4952-4958, doi:10.1175/JCLI-D-13-00628.1.

Roca, R. and Fiolleau, T., 2020. Extreme precipitation in the tropics is closely associated with long-lived convective systems. Communications Earth & Environment, 1(1), p.18, doi:10.1038/s43247-020-00015-4

Singleton, A. and Toumi, R., 2013. Super‐Clausius–Clapeyron scaling of rainfall in a model squall line. Quarterly Journal of the Royal Meteorological Society, 139(671), pp.334-339, doi:10.1002/qj.1919

Schumacher, R.S. and Rasmussen, K.L., 2020. The formation, character and changing nature of mesoscale convective systems. Nature Reviews Earth & Environment, 1(6), pp.300-314, doi:10.1038/s43017-020-0057-7

Sun, Q., Zhang, X., Zwiers, F., Westra, S. and Alexander, L.V., 2021. A global, continental, and regional analysis of changes in extreme precipitation. Journal of Climate, 34(1), pp.243-258, doi:10.1175/JCLI-D-19-0892.1

Thackeray, C.W., Hall, A., Norris, J. and Chen, D., 2022. Constraining the increased frequency of global precipitation extremes under warming. Nature Climate Change, 12(5), pp.441-448, doi:10.1038/s41558-022-01329-1

U.S. Global Change Research Program, 2023, Fifth National Climate Assessment, doi: 10.7930/NCA5.2023

Wang, T., Li, Z., Ma, Z., Gao, Z. and Tang, G., 2023. Diverging identifications of extreme precipitation events from satellite observations and reanalysis products: A global perspective based on an object-tracking method. Remote Sensing of Environment, 288, p.113490, doi:10.1016/j.rse.2023.113490

Westra, S., Fowler, H.J., Evans, J.P., Alexander, L.V., Berg, P., Johnson, F., Kendon, E.J., Lenderink, G. and Roberts, N., 2014. Future changes to the intensity and frequency of short‐duration extreme rainfall. Reviews of Geophysics, 52(3), pp.522-555, doi:10.1002/2014RG000464

Willeit, M., Amorati, R., Montani, A., Pavan, V. and Tesini, M.S., 2015. Comparison of spectral characteristics of precipitation from radar estimates and COSMO-model predicted fields. Meteorology and Atmospheric Physics, 127, pp.191-203, doi:10.1007/s00703-014-0359-8

Williams, A.P., McKinnon, K.A., Anchukaitis, K.J., Gershunov, A., Varuolo-Clarke, A.M., Clemesha, R.E. and Liu, H., 2024. Anthropogenic intensification of cool-season precipitation is not yet detectable across the Western United States. Journal of Geophysical Research: Atmospheres, 129(12), p.e2023JD040537, doi:10.1029/2023JD040537

Zaitchik, B.F., Rodell, M., Biasutti, M. and Seneviratne, S.I., 2023. Wetting and drying trends under climate change. Nature Water, 1(6), pp.502-513, doi:10.1038/s44221-023-00073-w

Zhao, M., 2022. A study of AR-, TS-, and MCS-associated precipitation and extreme precipitation in present and warmer climates. Journal of Climate, 35(2), pp.479-497, doi:10.1175/JCLI-D-21-0145.1

Geophysical Review Letters

Supporting Information
for
The fine-scale signature of precipitation intensification trends in the CONUS-404 hydroclimate reanalysis between 1993 and 2022

Clément Guilloteau[1],*, Xiaodong Chen[2,3], L. Ruby Leung[4], and Efi Foufoula-Georgiou[1,5]

[1] Department of Civil and Environmental Engineering, University of California Irvine

[2] School of Meteorology, University of Oklahoma, Norman

[3] School of Civil Engineering and Environmental Science, University of Oklahoma, Norman

[4] Atmospheric, Climate and Earth Sciences Division, Pacific Northwest National Laboratory, Richland, Washington

[5] Department of Earth System Science, University of California Irvine

* corresponding author, cguillot@uci.edu

Contents of this file

Figures S1 and S2.

Introduction

The two supplementary figures demonstrate that the p-values derived with three different methods, namely, t-test, Mann-Kendall test and Monte Carlo permutations (with *N=500* permutations) are consistent with each-other regarding the statistical significance of the trends in the annual frequency of wet hours at 4-km resolution (Figure S1) and in the mean annual wet-hour intensity at 4-km resolution (Figure S2) across the 7477 surfels of dimension of the CONUS study domain. In particular, the statistical distributions (CDFs) of the p-values across the domain are found quasi-identical, regardless of the method.

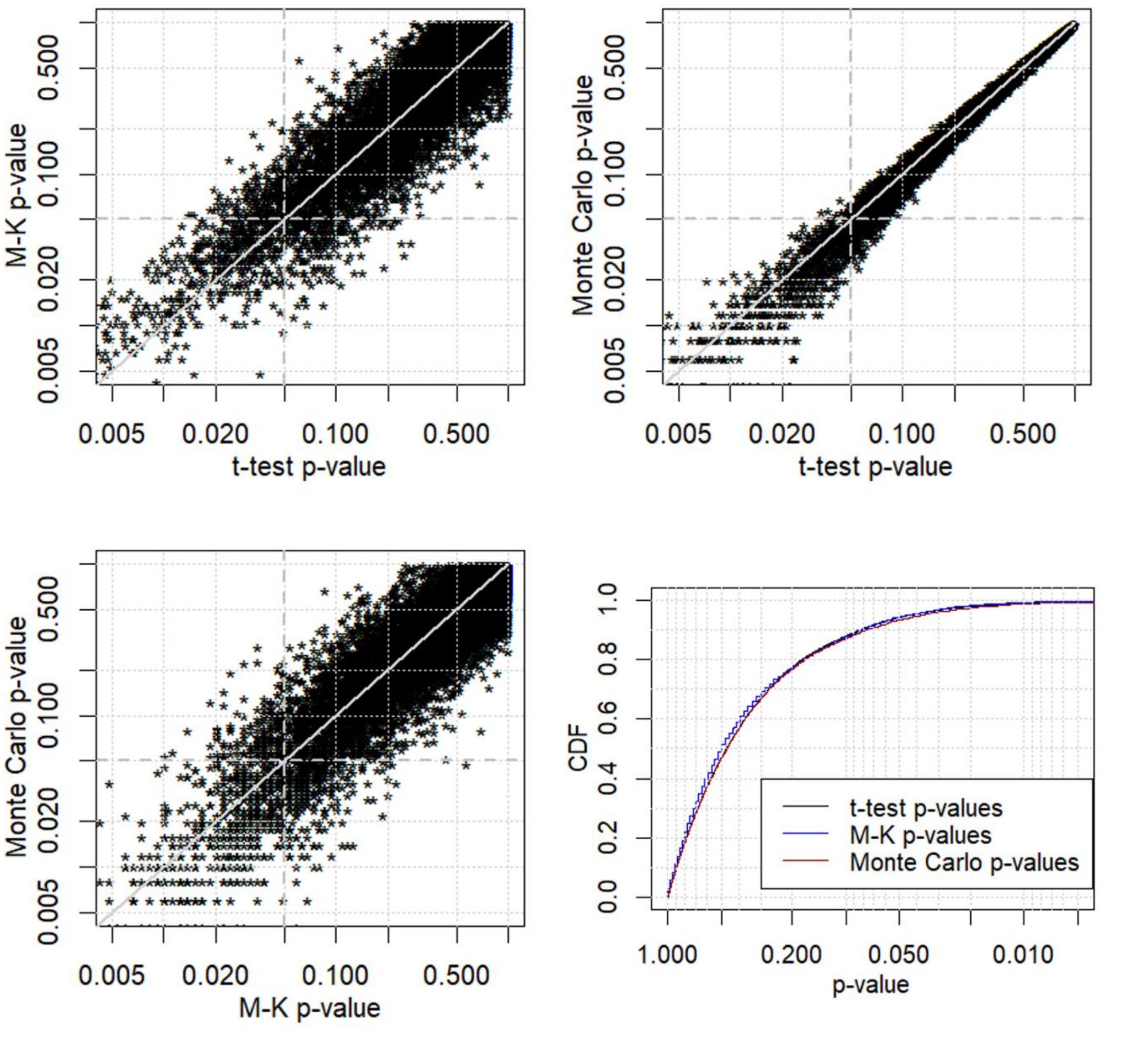

Figure S1: Comparison of the p-values derived from different tests, namely, t-test, Mann-Kendall (M-K) test and, Monte-Carlo permutation of the time series (with N=500 permutations), for the trends in the 1993-2022 time series of annual frequency of wet hours at 4 km resolution across the 7477 surfels of dimension 40 km by 40 km of the study domain. (a) Scatter plot, M-K test against t-test. (b) Scatter plot, Monte Carlo permutations against t-test. (c) Scatter plot, Monte Carlo permutations against M-K test. (d) Cumulative distribution functions (CDF) of the 7477 p-values for the three tests (note that the p-values are in decreasing order on the x-axis).

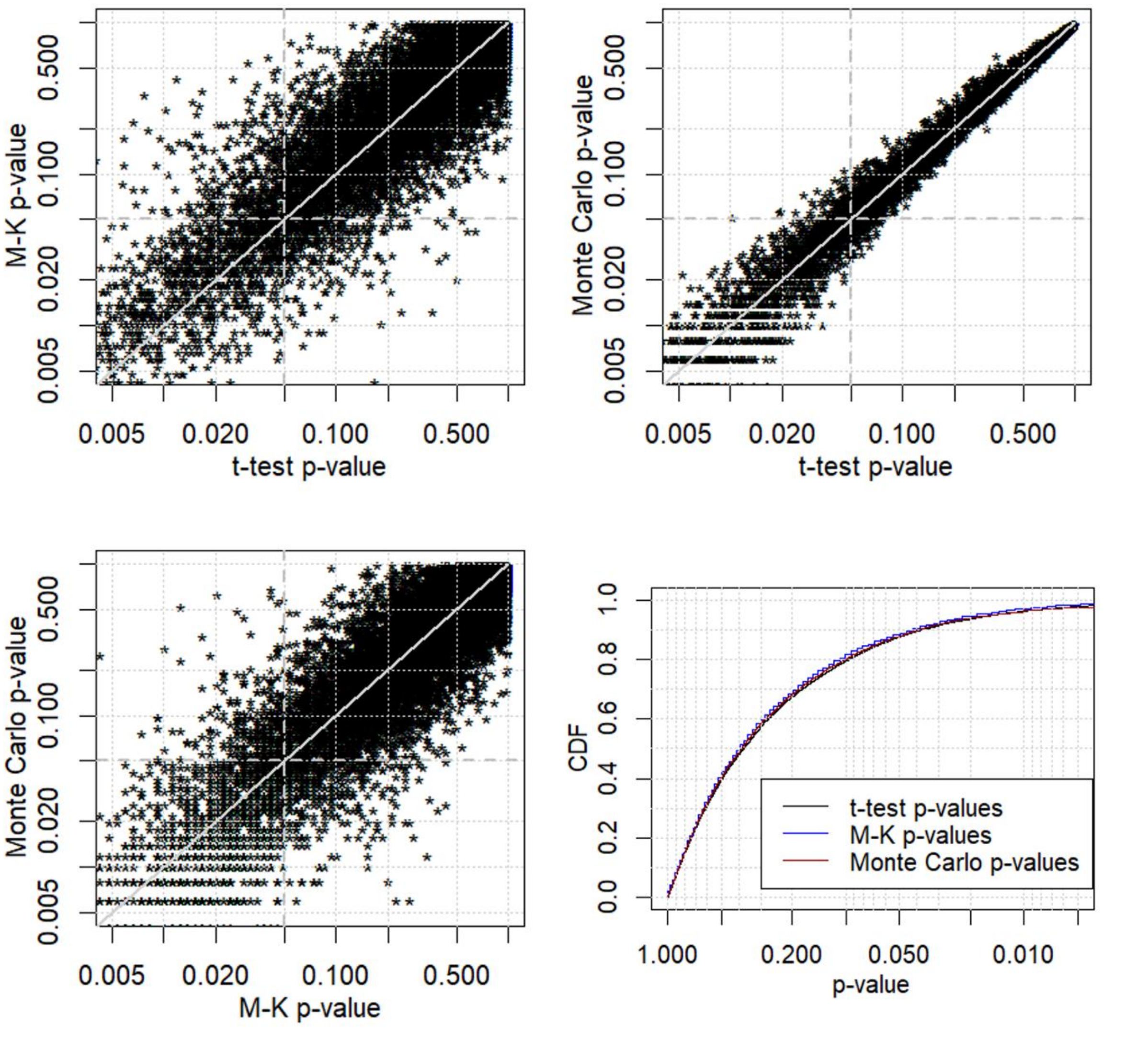

Figure S2: Comparison of the p-values derived from different tests, namely, t-test, Mann-Kendall (M-K) test and, Monte-Carlo permutation of the time series (with *N*=500 permutations), for the trends in the 1993-2022 time series of annual mean wet-hour intensity at 4 km resolution across the 7477 surfels of dimension 40 km by 40 km of the study domain. (a) Scatter plot, M-K test against t-test. (b) Scatter plot, Monte Carlo permutations against t-test. (c) Scatter plot, Monte Carlo permutations against M-K test. (d) Cumulative distribution functions (CDF) of the 7477 p-values for the three tests (note that the p-values are in decreasing order on the x-axis).